Journal of ELECTRONIC MATERIALS, Vol. 35, No. 12, 2006 *Regular Issue Paper*

Microstructural Characteristics and Vibration Fracture Properties of Sn-Ag-Cu-TM (TM = Co, Ni, and Zn) alloys

JENN-MING SONG,[1,2] CHI-FENG HUANG,[1] and HSIN-YI CHUANG[1]

1.—Department of Materials Science and Engineering, National Dong Hwa University, Hualien 974, Taiwan, Republic of China. 2.—E-mail: samsong@mail.ndhu.edu.tw

This study investigated microstructure, thermal behavior, and mechanical properties of Sn-3.3Ag-0.5Cu alloys (SAC) with the addition of transition metals (TM, Ni, Co, and Zn). Results show that alloying with TM elements was able to reduce the degree of undercooling and strengthen SAC alloys. Among these elements, only Zn can raise the ductility. CoSn and Cu-Ni-Sn intermetallics appeared, respectively, in the Co-containing and Ni-containing samples while coarse Sn dendrites and a large area of eutectic phases could be observed in the specimens with Zn. These microstructural changes led to an inferior vibration fracture resistance under resonant vibration with a constant pull force.

Key words: Lead-free solder, Sn-Ag-Cu, transition metals, resonant vibration, tensile properties

INTRODUCTION

Near-ternary eutectic Sn-Ag-Cu alloys are considered one of the most favorable systems as a lead-free solder. However, there are still some shortcomings that need to be overcome, for example, a somewhat higher melting temperature,[1] hot tearing due to coarse proeutectic Sn dendrites,[2] large Ag_3Sn plate and thus induced strain localization,[3] and excess growth of interfacial compounds.[4] Several alloying elements have been proposed for modifying the microstructure, thermal behavior, and interfaces of Sn-Ag-Cu joints. Numerous reports have indicated that In and Bi can be applied to reduce the melting points of Sn-Ag alloys.[5–7] Also, Sb and rare earths (RE) can significantly retard the growth of interfacial compounds during thermal aging.[8–10]

Recent research has revealed that additions of transition metals (TM) to Sn-Ag-Cu alloys provided a marked improvement in microstructural modification and mechanical properties and have attracted considerable attention. Anderson et al.[11,12] proposed that adding Co and Fe can effectively refine microstructure, reduce the degree of undercooling, modify interfacial Cu-Sn compounds, and increase the shear strength of joints with Cu. Kariya et al.[13] suggested that a very small amount of Ni addition (0.05 wt.%) can enhance the low cycle fatigue endurance of flip-chip interconnections. Also, it has been reported that for the joints of Ni-doped Sn-Ag solders and Cu, interfacial IMC was irregular $(Cu,Ni)_6Sn_5$ rather than scalloped Cu_6Sn_5 and did not show an observable change in thickness after long aging time.[14,15] Suganuma et al.[16] reported that TM elements (including Fe, Ni, Co, Mn, and Ti) can form various intermetallic compound (IMC) precipitates and reduce undercooling in solidification to varying extents. Kang et al.[17] demonstrated that a minor Zn addition has the ability to reduce undercooling efficiently and suppress the formation of massive primary Ag_3Sn plates. It was also found that Zn can retard the growth of Cu-Sn compounds at Sn-Ag-Cu/Cu interfaces suffering multiple reflow cycles and solid-state annealing.[18,19]

To further understand the effect of TM additions on the microstructure and mechanical properties, in this study near-eutectic Sn-Ag-Cu-X (X = Ni, Co, and Zn) were prepared to investigate the relationships between solidification structure and thermal and tensile properties. Additionally, the vibration fracture resistance of solders is of importance when joints are assembled, e.g., in vehicles and aircraft,[20,21] and is apparently influenced by the microstructural features. Therefore, vibration tests were also performed to evaluate the effect of TM additions on the mechanical performance of Sn-Ag-Cu alloys. The vibration properties examined included the vibration fracture resistance, crack propagation morphology, and ability to absorb vibration energy.

(Received April 19, 2006; accepted June 29, 2006)

EXPERIMENTAL PROCEDURES

The Sn-Ag-Cu-X alloys investigated were Sn-3.3 wt.% Ag-0.5 wt.% Cu alloy and those with 0.5 wt.% TM addition (Ni, Co, and Zn). The specimens are designated according to their compositions and are referred to as SAC, SAC-Ni, SAC-Co, and SAC-Zn. All the alloys were prepared by melting pure metal in a vacuum arc melting furnace and subsequently remelting and casting into a Y-shaped graphite mold. The average solidification rate was measured to be 16.7°C/sec. Excessive growth of primary intermetallic phase, Ag_3Sn, could be prevented under this cooling condition.

All the specimens were soaked in an oil bath at 120°C for 1 h to stabilize the microstructure before testing. Using an image analyzer, the microstructural characteristics, secondary dendrite arm spacing (SDAS) of Sn, and the area fraction of individual phase were analyzed quantitatively. Each datum was the average of 15 observations. A scanning electron microscope (SEM) and an electron probe microanalyser (EPMA) were used to observe and analyze the microstructure.

The thermal behavior of the alloys was investigated using differential scanning calorimetry (DSC) analysis. The specimens were heated up to above 300°C and then cooled to the ambient temperature, with a constant rate of 1°C/min.

To collect tensile data for reference, rectangular specimens (gauge length section: 20 mm × 5 mm × 2 mm) were also prepared to perform tensile tests (initial strain rate: 7.5×10^{-4} s^{-1}). Each datum was the average of five tests or more.

A simple cantilever beam vibration system, shown schematically in Fig. 1a, was used for the vibration experiments. The graphite cast test specimen (Fig. 1b), rectangular with dimensions 20 mm × 100 mm × 4 mm, was mounted and fixed on end to the vibration shaker. Two V-notches near the clamp were made to restrict crack initiation from the notch front. The vibration force was monitored using an acceleration sensor, and the deflection amplitude of the specimen at the end opposite the vibration shaker was detected by a deflection sensor once a second. The resonant vibration tests were conducted with a fixed vibration force (2G, where G denotes the acceleration due to gravity, $9.8 m/s^2$) at the resonant frequency. The resonant vibration tests were conducted at the resonance frequency, which was taken as the frequency leading to the largest deflection and determined by varying the vibration frequency continuously. The variation in deflection amplitude against the number of vibration cycles was recorded. Each datum was the average of results from more than 3 samples.

To understand the crack propagation due to vibration deformation, crack tortuosity, defined as the ratio of the length of the main crack to the projected length of this crack along the transverse direction of the specimen, was quantified (Fig. 2). Each datum was the average of results from 5 samples.

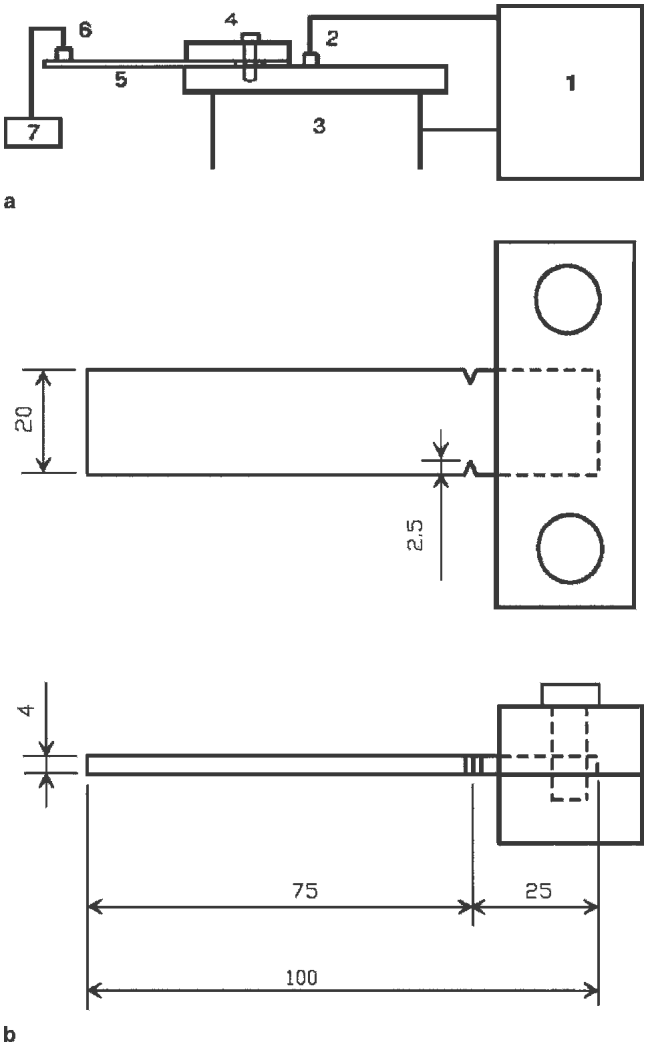

Fig. 1. (a) The vibration apparatus (1. vibration controller, 2. acceleration sensor, 3. vibration shaker, 4. specimen clamp, 5. specimen, 6. deflection sensor, 7. recorder). (b) The dimension of test specimens (unit: mm).

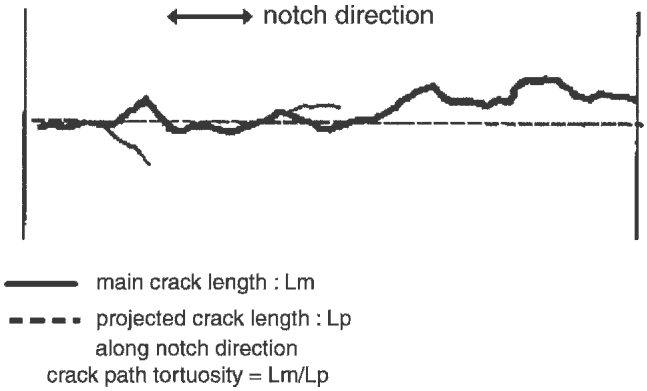

Fig. 2. Definition of crack tortuosity.

Damping capacity was measured in terms of logarithmic decrement (δ value), which was derived from the deflection amplitude decay of a specimen under free vibration. Logarithmic decrement value is defined as follows:[22]

$$\delta = 1/n \ln (A_i/A_{i+n})$$

where A_i and A_{i+n} are the deflection amplitude of the ith cycle and the (i + n)th cycle separated by n periods of oscillation.

RESULTS

Microstructural Feature and Thermal Properties

Figure 3 shows the microstructure of the specimens investigated. As illustrated, Sn dendrites and the interdendritic regions with eutectic phases composed of Sn, Ag_3Sn, and Cu_6Sn_5 could be observed. The Sn dendrites became finer with the addition of Ni or Co, while the SAC-Zn samples possessed coarser Sn dendrites and, remarkably, a larger area of eutectic phases. The quantitative data of the microstructural changes are listed in Fig. 4. In addition to the intermetallics of ternary eutectic phases Ag_3Sn and Cu_6Sn_5, additional compound particles resulting from alloying, named heterogeneous IMCs, can be clearly observed in the SAC-Ni and SAC-Co samples (Fig. 3b and 3c). The area fraction of these heterogeneous compounds was about 5% for both the Ni-containing and Co containing specimens. Figures 5–7 display the magnified structure of the samples. In addition to finer Sn dendrites, the IMC particles in the interdendritic regions of the SAC-Ni samples were less packed compared to those of the SAC (Fig. 5a and 5b). Cu-Ni-Sn compounds with dendritic or chunky appearance were dispersed mainly within the ternary eutectic regions (Fig. 5b). EPMA analysis results (Fig. 5c) reveal that those compounds can be distinguished into $(Cu_{0.61},Ni_{0.39})_6Sn_5$ and $(Ni_{0.84},Cu_{0.16})_3Sn_4$. Figure 6 illustrates the enlarged structure of the SAC-Co sample, which shows numerous acicular and rectangular intermetallics. The morphology and composition of these compounds (Fig. 6b), reveal that the main intermetallic phase was $CoSn_2$. In addition, a high Co phase,

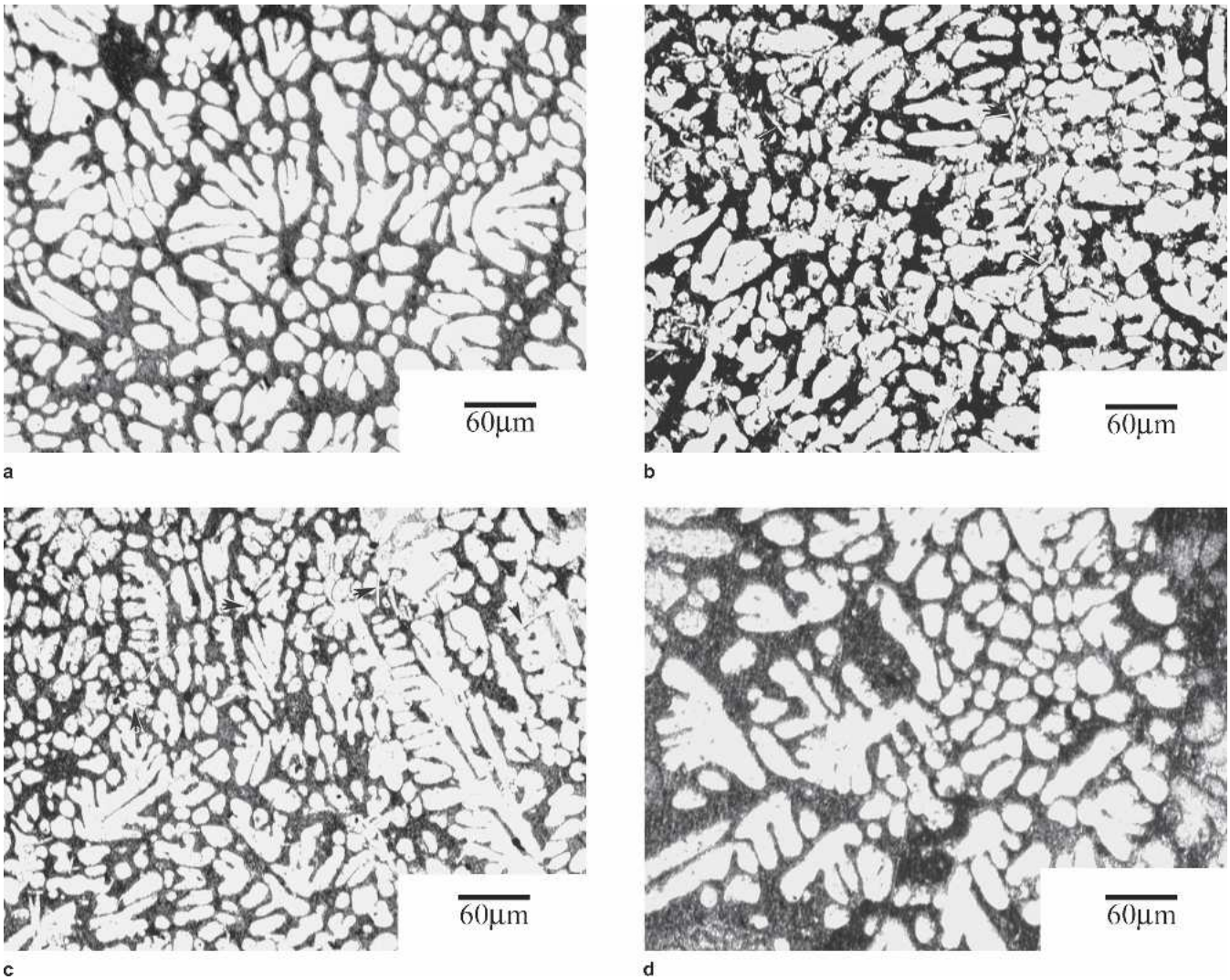

Fig. 3. Microstructures of the specimens: (a) SAC, (b) SAC-0.5Ni, (c) SAC-0.5Co, and (d) SAC-0.5Zn (heterogeneous compounds are indicated by arrows).

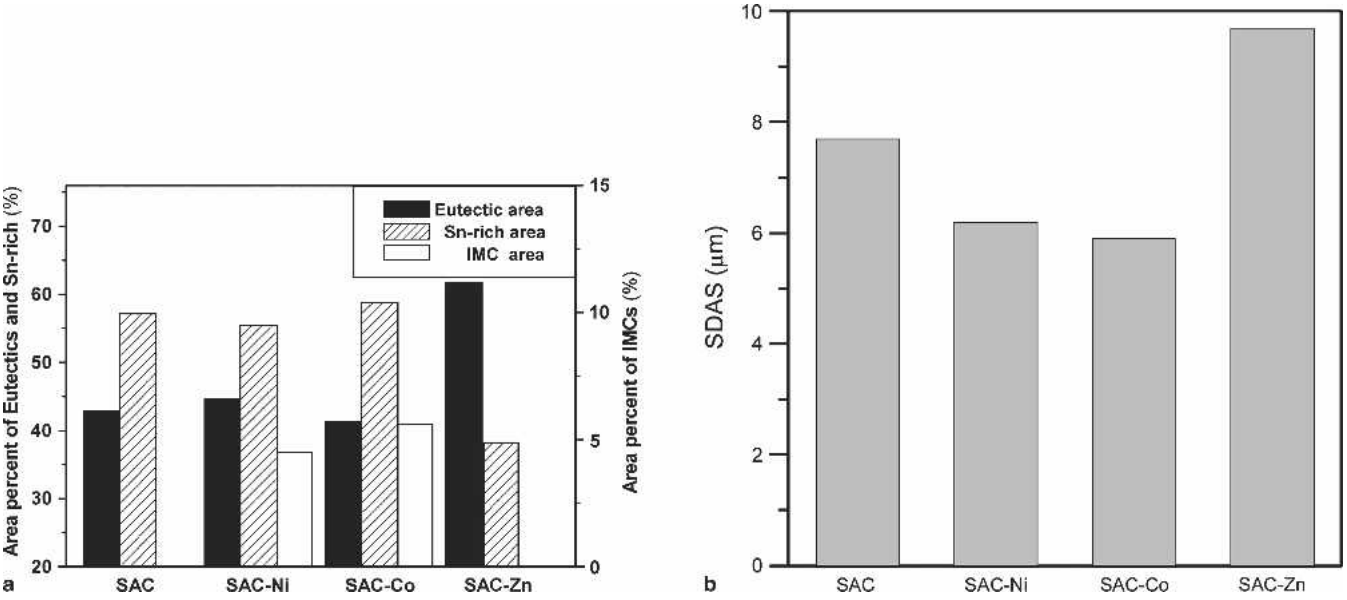

Fig. 4. Quantitative data of the microstructure of the specimens: (a) area fractions of the phases and (b) secondary dendrite arm spacing (SDAS) of Sn dendrites.

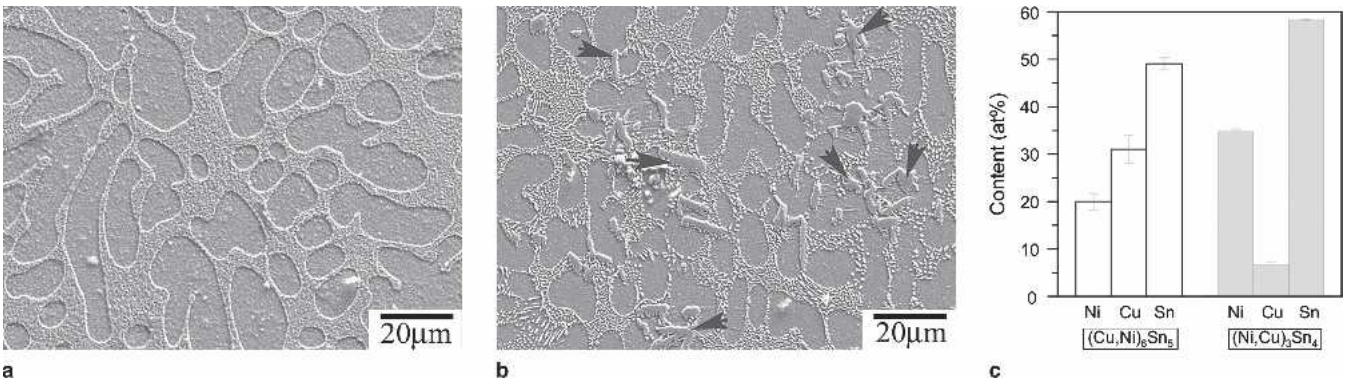

Fig. 5. Magnified structure of (a) the SAC and (b, c) the SAC-Ni samples and the compositions of Cu-Ni-Sn IMCs pointed out by arrows.

CoSn, and an unreported low Co phase with about 10 at.% Co could also be observed. The $CoSn_2$ surrounding CoSn can be considered as the reaction product of a peritectic transformation, L + CoSn → $CoSn_2$.[23] Figure 7 shows that Sn dendrites became coarse in the Zn-added samples. Interestingly, a very small amount of Zn-rich phase (Fig. 7b) of composition Zn-9–20%Sn, could be found within the interdendritic regions. In addition, Zn atoms were also detected to segregate at the interdendritic regions (Fig. 7c and 7d).

To further understand the microstructural differences caused by alloying TM elements, the thermal behavior of the specimens was also examined. Figure 8 shows the DSC endothermic and exothermic peaks of the samples used upon heating and cooling respectively. Figure 8a reveals that upon heating, the temperatures of the endothermal peaks for the eutectic reaction of the samples did not differ very much, and that of the SAC-Zn specimen was slightly lower than the others. Due to undercooling, the exothermic peaks upon cooling for all the samples appeared at a lower temperature compared to their endothermal peak, but the reductions in temperature were not identical (Fig. 8b). Remarkably, the exothermic peaks for the samples with TM additions were observed at higher temperatures than the unalloyed sample, especially for SAC-Zn and SAC-Co. The transition points for each specimen, the onset temperature of the endothermic peaks (which was regarded as the melting point), as well as the peak temperatures of endothermic and exothermal reactions and their difference representing degree of undercooling, are shown in Fig. 9. It is worth noting that the degree of undercooling decreased in turn from SAC, SAC-Ni, SAC-Co, to SAC-Zn. The SAC-Zn sample exhibited a drastically reduced undercooling of only 5.2°C.

Tensile Properties and Performance Under Resonance

Figure 10 lists the tensile properties, elongation to failure, yield strength, and ultimate tensile strength

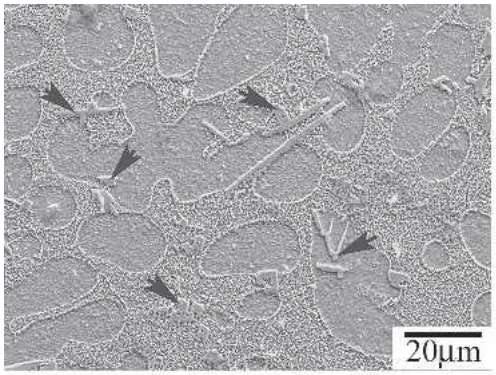

a

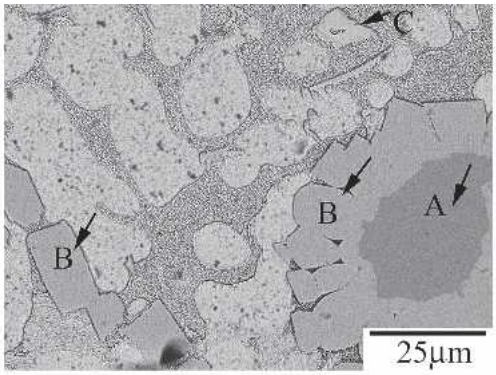

b

Element	A	B	C
Co	45.68	27.58	10.64
Sn	54.32	72.42	89.36

c

Fig. 6. (a) Magnified structure of the SAC-Co and (b) the morphology and composition (in at.%) of the CoSn compounds.

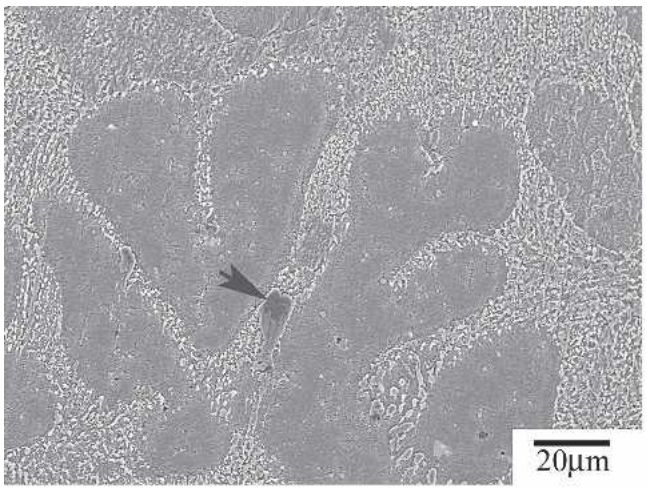

a

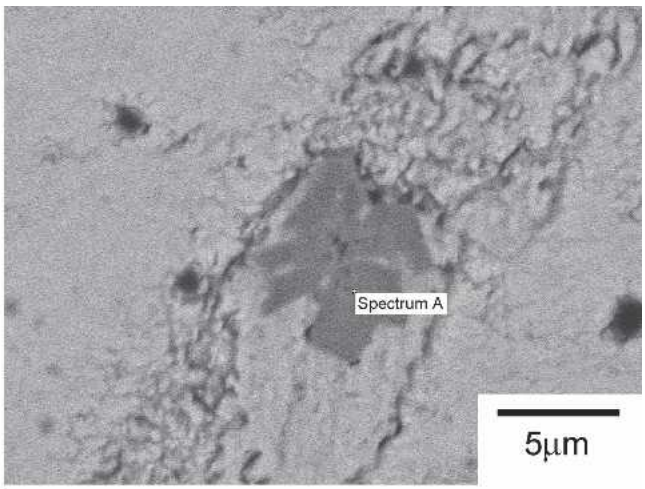

b

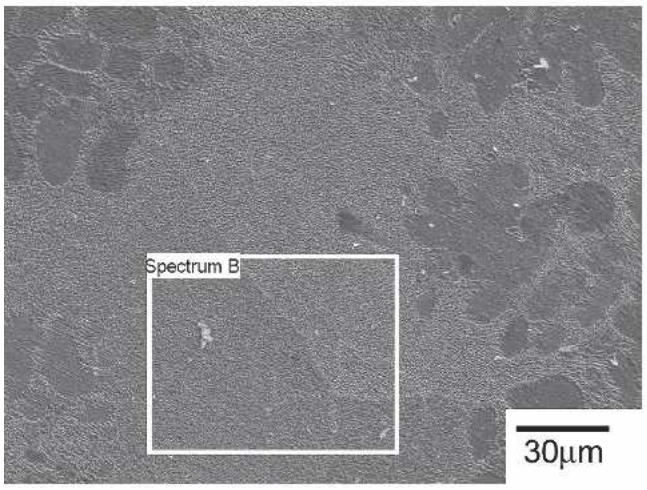

c

	Zn	Cu	Ag	Sn
A	84.46	—	—	15.54
B	5.54	2.81	7.54	84.12

d

Fig. 7. (a) Magnified structure of the SAC-Zn, (b) the Zn-rich phase, (c) the extended eutectic region, and (d) the compositions (in at.%) of point A in (b) and area B in (c).

of the specimens. We see that the Ni-containing and Co-containing alloys have a greater tensile strength and lower ductility than the SAC alloy. It is worth noting that with 0.5 wt.% Zn, a combination of improved strength and greater elongation could be obtained. Cross-sectional structure shown in Fig. 11 illustrates that heterogeneous IMCs including CoSn and Cu-Ni-Sn intermetallics were well-bonded with the matrix, and no decohesion of the particle-matrix interface could be observed in the severely deformed region near fracture surface. It could also be found that fracturing tended to propagate along those

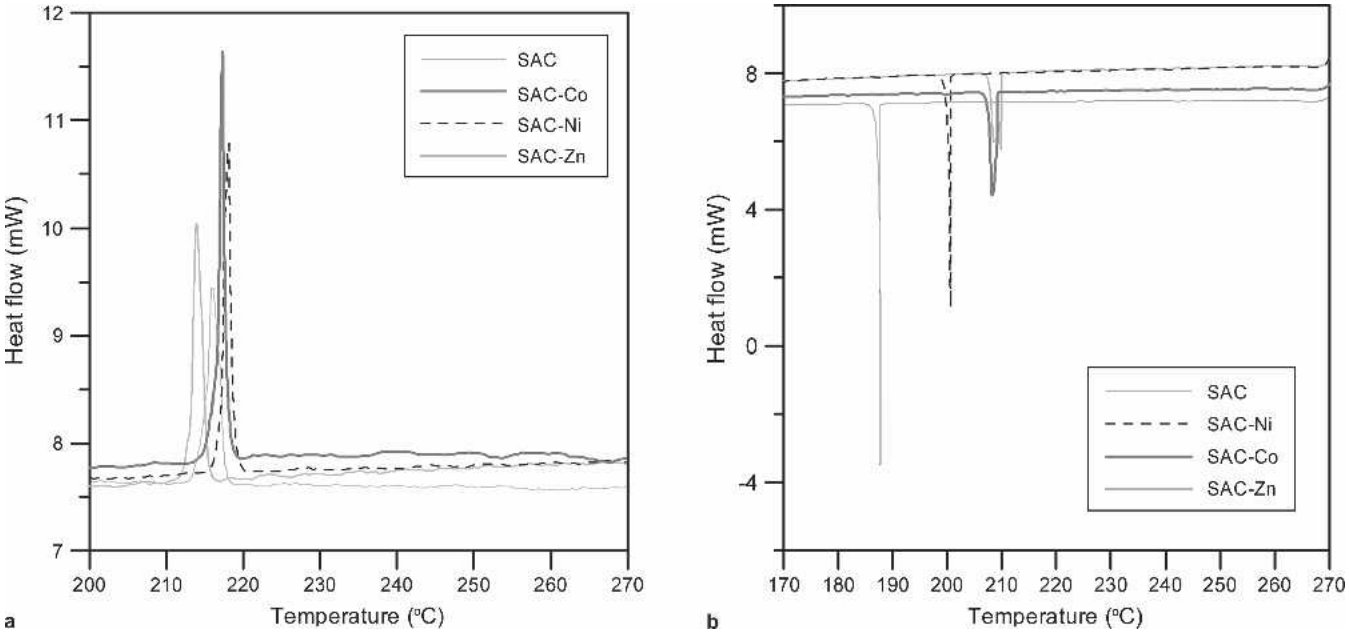

Fig. 8. DSC analysis results: (a) upon heating and (b) upon cooling.

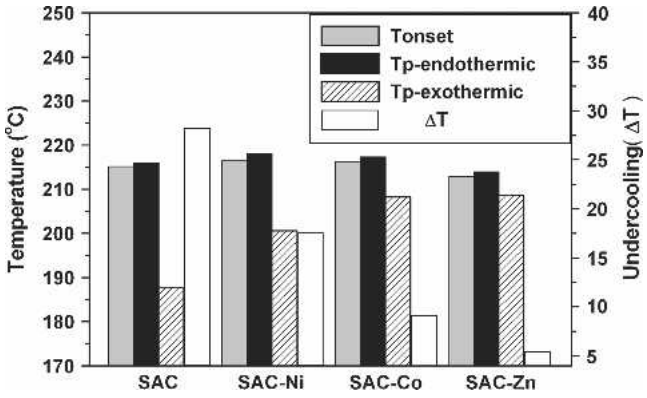

Fig. 9. Transition points and the degree of undercooling estimated from Fig. 8 (Tp-endothermic and Tp-exothermic are ultimate temperature value of the endothermic peaks upon heating and exothermic peaks upon cooling; Tonset is the onset point of heat absorption upon heating).

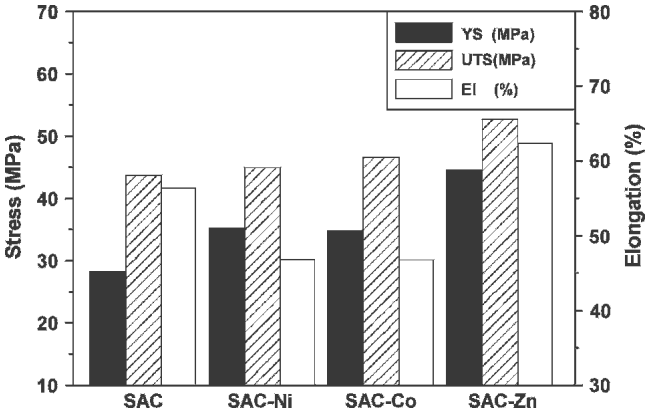

Fig. 10. Tensile strength and elongation of the samples (UTS: ultimate tensile strength; YS: yield strength; EL: total elongation).

heterogeneous IMCs. Some fragmented IMCs were observed on the fracture surface.

The dependence of deflection amplitude on the number of vibration cycles (D-N curve) for a fixed vibration force of 2G is shown in Fig. 12a. The frequencies applied in each case are shown in Table I. Those are 80 Hz for the SAC, 78 Hz for the SAC-Ni, and 82 Hz for both the SAC-Co and SAC-Zn specimens. After a short initial ascending stage caused by strain hardening, the deflection amplitude remained nearly constant with increasing vibration cycles, but subsequently, the deflection amplitude decreased with increasing vibration cycles due to the deviation of the actual vibration frequency from the resonant frequency caused by the inward propagation of major cracks.[24] Therefore, the vibration life of a sample can be defined as the number of cycles at the beginning of descending deflection amplitude.

As illustrated in Fig. 12b, the vibration life (critical cyclic number to failure) in decreasing order was SAC, SAC-Ni, SAC-Zn, and SAC-Co, while that for initial deflection amplitude was SAC-Zn, SAC-Co, SAC, and then SAC-Ni. According to the measured logarithmic decrement (Table I) and the data of initial deflection, it can be derived that the deflection amplitude of the specimens is inversely proportional to the damping capacity (Fig. 13). However, there seems to be no direct correlation between damping capacity and vibration life. This will be discussed later.

Results of microstructural observation on the samples' surface after vibration test are shown in Fig. 14. It reveals that a deformation zone appeared around the main crack in-between the two V notches of the specimen. Figure 14b displays that the vibration-deformed structure was observed only within Sn-rich dendritic regions and exhibited a striated

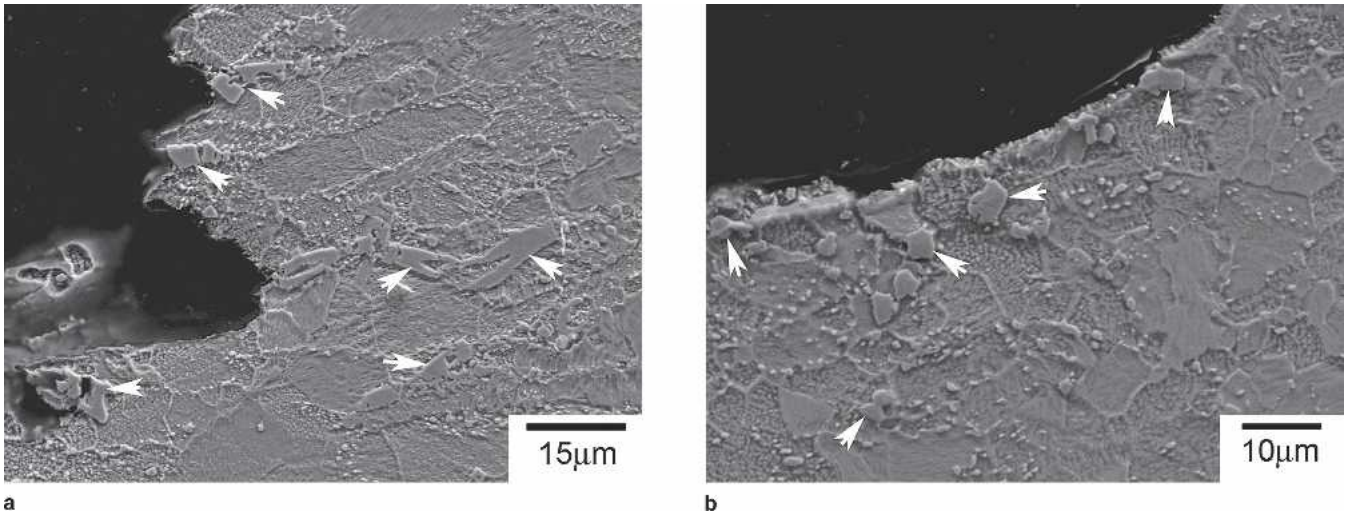

Fig. 11. Cross-sectional images of the fractured tensile specimens with heterogeneous IMCs: (a) SAC-Co and (b) SAC-Ni (IMCs are indicated by arrows).

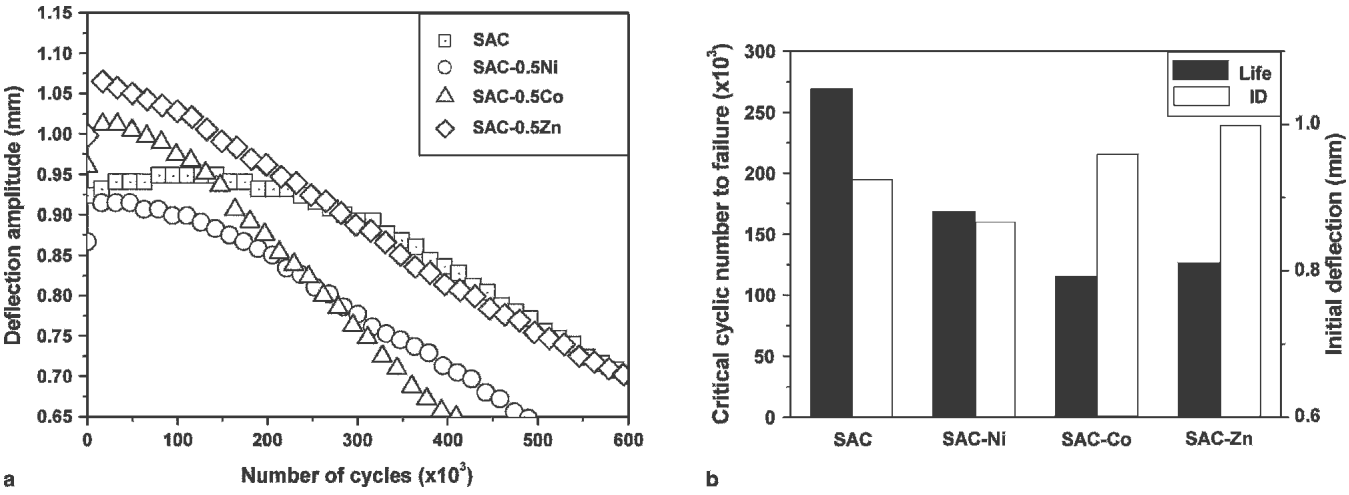

Fig. 12. (a) D-N curves of the samples under a fixed vibration force of 2G and (b) initial deflection amplitude and vibration life estimated from (a).

Table I. Resonant Frequencies and Logarithmic Decrements of the Specimens.

Sample	Resonant Frequency (Hz)	δ value ($\times 10^{-3}$)
SAC	80 ± 1	15.8
SAC-0.5Ni	78 ± 1	17.1
SAC-0.5Co	82 ± 1	15.0
SAC-0.5Zn	82 ± 1	14.4

deformation pattern. It was found that the SAC-Zn sample (Fig. 14e) had a smaller number of these white regions than the others. The tortuosity of the main crack remained constant for the SAC and SAC-Ni samples but was relatively lower for the SAC-Co and SAC-Zn specimens (Table II).

Detailed observation (Fig. 15) showed that the main crack tended to grow through or along the broken massive compounds (Cu-Ni-Sn or CoSn). Some broken IMCs were also found embedded in the vibration-deformed regions (Fig. 16).

DISCUSSION

Effect of TM Alloying on the Microstructure

It has been reported that the addition of transition metals can reduce the undercooling of Sn-Ag-Cu alloys and also leads to an improved strength.[16,17] Microstructural observation results (Figs. 3–7) show that Co and Ni formed additional intermetallics rather than inherent Ag_3Sn and Cu_6Sn_5 of Sn-Ag-Cu eutectic alloys. These heterogeneous IMCs might act as heterogeneous nucleation sites for Sn dendrites upon solidification and thus reduce the undercooling requested. A previous report reveals that hypereutectic SAC alloys with primary Cu_6Sn_5 show the same phenomenon.[25] The heterogeneous nucleation speculation could also explain the refined structure of the SAC-Ni and SAC-Co alloys.

Zn also has a great effect on suppressing the undercooling. Kang et al.[17] reported that Zn segregated with the eutectic phases and may have formed Zn containing IMCs with Cu. However, in this study a high Zn phase (Zn content was about 80 at.%) was

observed within the interdendritic regions. The addition of Zn led to a more equilibrium solidification of SAC alloys, and this is evidenced by the increased area fraction of eutectic phases. However, the mechanism to reduce undercooling required for crystallization of Sn dendrites for SAC-Zn alloys is not identical to those with other elements and needs further investigation.

Role of Structural Phases on Mechanical Properties

It has been demonstrated that in Sn-Ag-Cu solder balls and at the joints Sn grain sizes are quite large and are strongly affected by the composition and cooling rate.[26–29] Cyclic growth twinning could be observed in the alloys with a near ternary eutectic composition.[28] Also, the degree of anisotropy of Sn grains is closely related to the mechanical behavior of the solder joints.[26] However, previous studies have proved that striated deformation in the Sn-rich phase plays an important role in absorbing vibration energy for Sn base solder alloys.[24,25,30] The size of Sn dendrite arms and the distribution of second phases dispersed in the Sn matrix are the dominant factors. Therefore, we discuss these two factors rather than size and orientation of Sn grains.

The striated deformation of the Sn-rich phase was caused by the extrusion-intrusion of the complex slip planes of the body-centered tetragonal (bct) Sn under high-frequency cyclic stress.[31] Because of the unequilibrium crystallization feature, Sn-Ag alloys exhibit an off-eutectic structure. As illustrated in Fig. 14b, striated deformation occurs easily in Sn dendrites. Based on the Granato-Lücke theory,[32] easier dislocation movement will lead to a higher damping capacity.

Microstructural refinement and formation of heterogeneous IMCs caused by addition of Ni and Co significantly affect the vibration properties of Sn-Ag-Cu alloys. The size reduction of the Sn dendrites caused by Co and Ni was considered to restrict the striated deformation and stunted dislocation slip. On the other hand, interfaces between heterogeneous

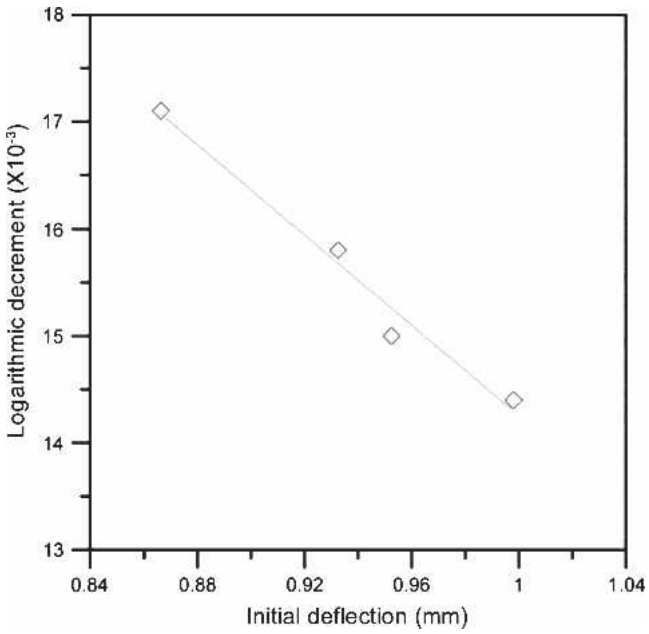

Fig. 13. Relationship between damping capacity and initial deflection.

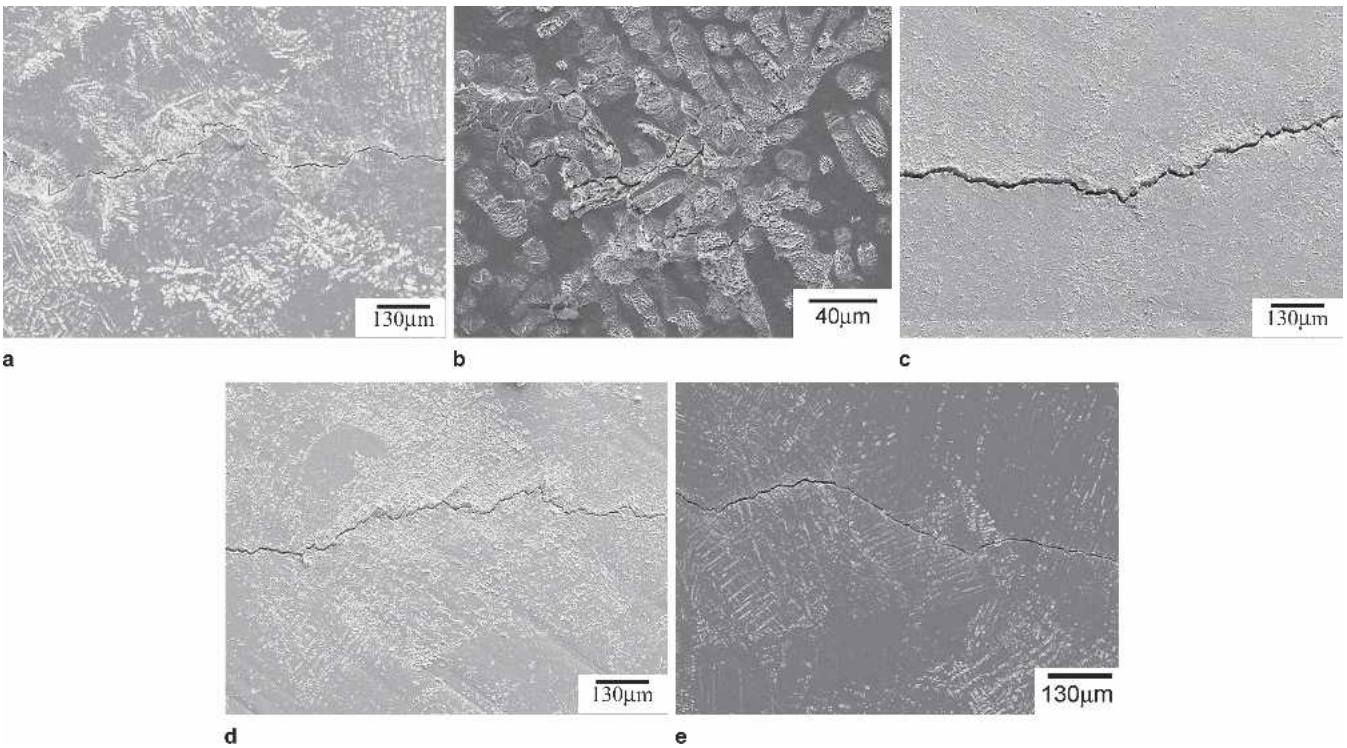

Fig. 14. Surface morphology of vibration-deformed specimens: (a) SAC, (b) enlarged image of (a), (c) SAC-Ni, and (d) SAC-Co, and (e) SAC-Zn.

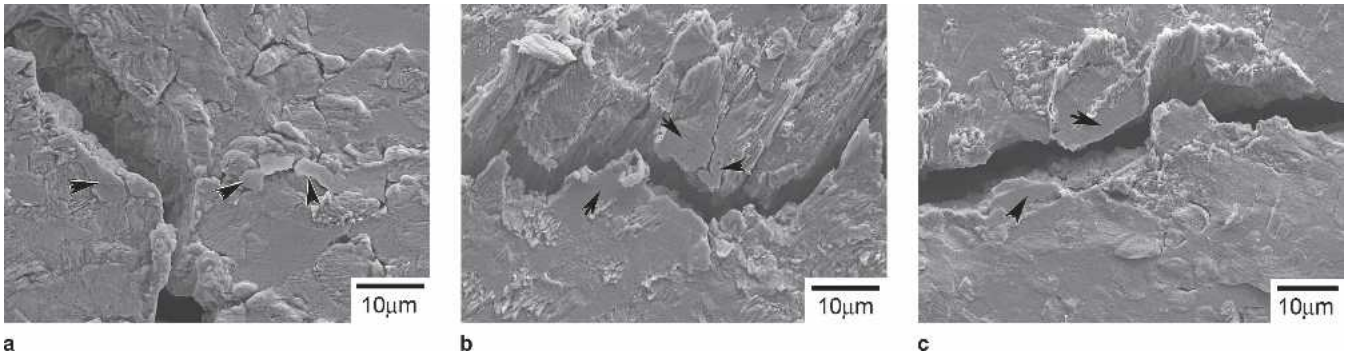

Fig. 15. Broken compounds, indicated by arrows, in vibration deformed structure of the (a) SAC-Ni and (b, c)SAC-Co samples.

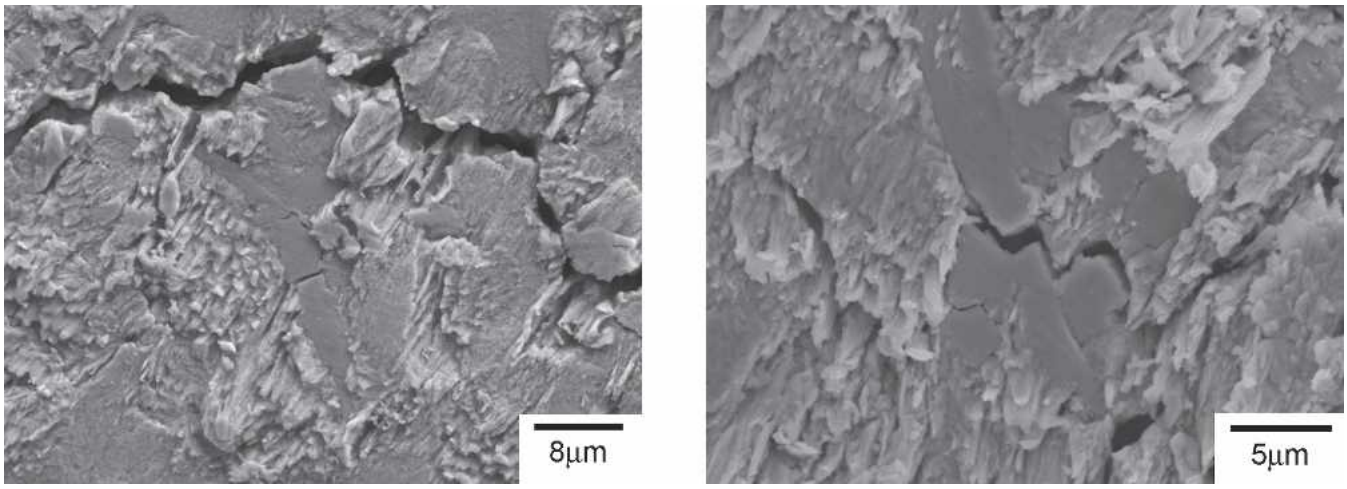

Fig. 16. Broken IMCs embedded in the vibration deformed structure of the samples: (a) the SAC-Ni and (b) the SAC-Co.

compounds and Sn matrix contribute to more internal friction and thus greater damping capacity. In the case of the SAC-Co sample, the effect of grain refining was dominant and resulted in a subsequently lower damping capacity and higher initial deflection. As for the SAC-Ni, one more factor should not be ignored: a less dense IMC distribution in the interdendritic regions, which may lower the deformation resistance of Sn in these regions. The dispersed eutectic phases combined with the presence of Cu-Ni-Sn compounds overcame the negative influence by microstructural refining and led to the greater damping capacity of SAC-Ni alloys.

The nature of massive intermetallics affects crack propagation.[24,25] Breakdown of IMCs during vibration will acceletare the crack growth. On the other hand, IMCs which do not break severely are advantageous to vibration fracture resistance. In this study, heterogeneous IMCs, Cu-Ni-Sn, and CoSn collapsed when suffering vibration deformation. The main crack tended to pass through the broken compounds and resulted in quick cracking and reduced vibration fracture resistance. This can explain why the critical cycles to failure and damping capacity did not show a linear relationship.

Table II. Crack Tortuosity of the Specimens (error value: ±0.01)

Sample	Tortuosity
SAC	1.12
SAC-Ni	1.12
SAC-Co	1.06
SAC-Zn	1.07

In spite of the coarse Sn dendrites, the SAC-Zn samples exhibited an inferior damping capacity. This can be ascribed to the large area of eutectic phases resulting from solidification more at equilibrium than the others. Furthermore, the higher eutectic area caused by Zn additions has a positive influence on the tensile strength without reducing elongation. Heterogeneous IMCs and their accompanying refining structure also hardened the alloys but the strengthening effect is inferior to the widely distributed eutectic network of the SAC-Zn. The existence of the CoSn and Cu-Ni-Sn particles did degrade the ductility. However, the SAC-Co and SAC-Ni specimens still possessed elongation greater than 40% due to good bonding between the IMCs and Sn matrix.

CONCLUSIONS

Transition metal additives Co, Ni, and Zn (0.5 wt.%) were individually applied to modify the eutec-

tic Sn-Ag-Cu alloy in this study. The influence on microstructure, thermal behavior, and mechanical properties of are summarized as follows:

- Addition of Co and Ni gives rise to the refinement of Sn-rich dendrites and the formation of heterogeneous intermetallics, several CoSn compounds, $(Cu,Ni)_6Sn_5$, and $(Ni,Cu)_3Sn_4$. Zn has a tremendously different contribution to the microstructure. Without forming IMCs, coarse Sn dendrites and an increased area fraction of eutectic phases, as well as a very small amount of Zn-rich phase, could be observed in the Zn-added alloys.
- All TM additions have the ability to reduce the degree of undercooling. SAC-Zn alloys possessed the smallest undercooling of only 5.2°C.
- With respect to tensile properties, SAC-Zn exhibits a combination of high tensile strength and great elongation. The specimens with Co and Ni have improved strength but decreased ductility. However, all the samples in this study possessed elongation of above 40%.
- The logarithmic decrement in decreasing order is SAC-Ni, SAC, SAC-Co, and SAC-Zn. The formation of Cu-Ni-Sn compounds and less-packed IMC distribution in the interdendritic regions gives rise to the greatest damping capacity of Ni containing alloys. Critical cyclic number to failure of the specimens decreases in turn from SAC, SAC-Ni, SAC-Zn, to SAC-Co. The breakdown of heterogeneous IMCs suffering vibration is probably responsible for the low vibration fracture resistance of SAC-Ni and SAC-Co samples. The worst damping capacity of the SAC-Zn alloy probably accounts for its short vibration life.

ACKNOWLEDGEMENT

This work was supported by the Chinese National Science Council (Contract No. NSC 94-2216-E-259-003), for which the authors are grateful.

REFERENCES

1. I.E. Anderson, B.A. Cook, J. Harringa, and R.L. Terpstra, *JOM* 54(6), 26 (2002).
2. G.S. Wable, S. Chada, B. Neal, and R.A. Fournelle, *JOM* 57(6), 38 (2005).
3. D.W. Henderson, T. Gosselin, A. Sarkhel, S.K. Kang, W.K. Choi, D.Y. Shih, C. Goldsmith, and K.J. Puttlitz, *J. Mater. Res.* 17, 2775 (2002).
4. D.R. Frear, J.W. Jang, J.K. Lin, and C. Zang, *JOM* 53(6), 28 (2001).
5. J. Zhao, L. Qi, X.M. Wang, and L. Wang, *J. Alloys Compd.* 375, 196 (2004).
6. P.T. Vianco and J.A. Rejent, *J. Electron. Mater.* 28, 1127 (1999).
7. A. Sharif and Y.C. Chan, *Thin Solid Films* 504, 431 (2006).
8. Z.G. Chen, Y.W. Shi, Z.D. Xia, and Y.F. Yan, *J. Electron. Mater.* 31, 1122 (2002).
9. C.M.L. Wu, D.Q. Yu, C.M.T. Law, and L. Wang, *J. Mater. Res.* 17, 3146 (2002).
10. B.L. Chen and G.Y. Li, *Thin Solid Films* 462-463, 395 (2004).
11. I.E. Anderson, J.C. Foley, B.A. Cook, J. Harringa, R.L. Terpstra, and O. Unal, *J. Electron. Mater.* 30, 1050 (2001).
12. I.E. Anderson, B.A. Cook, J. Harringa, and R.L. Terpstra, *J. Electron. Mater.* 31, 1166 (2002).
13. Y. Kariya, T. Hoso, T. Kimura, and S. Terashima, *The Inter Society Conference on Thermal Phenomena* (Piscataway, NJ: IEEE, 2004), pp. 103–108.
14. C.M. Chuang and K.L. Lin, *J. Electron. Mater.* 32, 1426 (2003).
15. C.M. Chuang, P.C. Shih, and K.L. Lin, *J. Electron. Mater.* 33, 1 (2004).
16. K.S. Kim, S.H. Huh, and K. Suganuma, *Microelectron. Reliab.* 43, 259 (2003).
17. S.K. Kang, D.Y. Shih, D. Leonard, D.W. Henderson, T. Gosselin, S. Cho, J. Yu, and W.K. Choi, *JOM* 56(6), 34 (2004).
18. S.K. Kang, D. Leonard, D.Y. Shih, L. Gignac, D.W. Henderson, S. Cho, and J. Yu, *J. Electron. Mater.* 35, 479 (2006).
19. D.J. Lee, D.H. Baek, K.K. Lee, K.M. Lee, and Y.J. Seo, *Z. Metallkd.* 96, 148 (2005).
20. Q.J. Yang, H.L.J. Pang, Z.P. Wang, G.H. Lim, F.F. Yap, and R.M. Lin, *Microelectron. Reliab.* 40, 1097 (2000).
21. Y.B. Kim, H. Noguchi, and M. Amagai, *Microelectron. Reliab.* 46, 459 (2006).
22. R.F. Steidel, Jr., *An Introduction to Mechanical Vibrations*, 3rd ed. (Hoboken, NJ: John Wiley & Sons, 1989), p. 169.
23. L. Liu, C. Andersson, and J. Liu, *J. Electron. Mater.* 33, 935 (2004).
24. J.M. Song, G.F. Lan, T.S. Lui, and L.H. Chen, *J. Alloys Compd.* 379, 233 (2004).
25. J.M. Song, F.I. Li, T.S. Lui, and L.H. Chen, *J. Mater. Res.* 19, 2665 (2004).
26. A.U. Telang, T.R. Bieler, S. Choi, and K.N. Subramanian, *J. Mater. Res.* 17, 2294 (2002).
27. A.U. Telang, T.R. Bieler, J.P. Lucas, K.N. Subramanian, L.P. Lehman, Y. Xing, and E.J. Cotts, *J. Electron. Mater.* 33, 1412 (2004).
28. L.P. Lehman et al., *J. Electron. Mater.* 33, 1429 (2004).
29. A. LaLonde, D. Emelander, J. Jeannette, C. Larson, W. Rietz, D. Swenson, and D.W. Henderson, *J. Electron. Mater.* 33, 1545 (2004).
30. C.M. Chuang, T.S. Lui, L.H. Chen, and T.M. Yin, *Mater. Trans.* 42, 2064 (2001).
31. J.S. Koehler, *Plastic Deformation in Crystallines Solids* (Pittsburgh, PA: Mellon Institute, 1950), p. 216.
32. A. Granato and K. Lücke, *J. Appl. Phys.* 27, 583 (1956).